

MODELING OF FLUCTUATING FLUID FORCES EXERTED ON THE WALLS OF A CONCENTRIC ANNULAR PIPE USING LARGE EDDY SIMULATION

S. Bhattacharjee^{1,2}, G. Ricciardi¹, and S. Viazzo²

¹: French Alternative Energies and Atomic Energy Commission (CEA) - Cadarache, DEN/DTN/STCP/LHC, 13108 St. Paul lez Durance Cedex, France

²: Laboratoire de Mécanique, Modélisation et Procédés Propres (M2P2), UMR7340 CNRS, Aix-Marseille Université, Centrale Marseille, 13451 Marseille Cedex, France
saptarshi.bhattacharjee@outlook.com; guillaume.ricciardi@cea.fr; stephane.viazzo@univ-amu.fr

ABSTRACT

Flow-induced vibrations in the pressurized water reactor core can cause fretting wear in fuel rods. This may damage the fuel rod cladding, thereby leading to a safety scenario. In order to ensure the integrity of the cladding, it is necessary to understand the fluid forces acting on the rods. In this paper, large eddy simulation was performed on a concentric annular pipe with mixing vanes: the inner wall represents the cladding. A hybrid structured-unstructured grid is used. Turbulent statistics for velocity and pressure were analyzed throughout the pipe. Effect of the vanes on the statistics was observed. Simulation results were compared with experimental and theoretical data. The swirl flow due to the vanes appears to be confined in the vicinity of the vanes.

KEYWORDS

LES, annular flow, CFD, fluid structure interaction, mixing vanes, wall pressure fluctuation

1. INTRODUCTION

Fuel rods in the core of a pressurized water nuclear reactor (PWR) are subjected to high axial fluid velocities of the order of 5m/s in order to ensure proper heat transfer. Typical PWR fuel assemblies consist of spacer grids fitted with springs and dimples to support the fuel rods. In addition, they are fitted with mixing vanes to generate strong swirls in the sub channels thereby improving the heat transfer. However, this high coolant velocity leads to vibrations in the fuel rods known as flow-induced vibrations (FIV). In such a situation, the flow is turbulent with Reynolds number $\sim 1 \times 10^5$. These vibrations can cause fretting wear in the fuel rods. In the US, 80% of the failures in PWRs, where thousands of hot irradiated fuel rods are cooled by fast-flowing water, are caused by grid-to-rod fretting (GRTF): a flow-induced vibration problem that leads to wear and failure of the rods [1]. Due to friction, fretting wear occurs at the contact points between the spacer grid and the fuel rod. This may compromise the first safety barrier of the nuclear reactor by damaging the fuel rod cladding. However it is not possible to do away with spacer grids [2]. So in order to ensure the integrity of the cladding, it is necessary to know the random fluctuating forces acting on the rods.

This paper presents large eddy simulation of flow around a rod in an annular cylindrical domain. This simplified domain serves as a first step towards studying fluctuating forces. The inner wall of the domain is representative of the fuel rod cladding. Also this geometry was chosen due to the availability of validation data: direct numerical simulation (DNS) results by Chung et al. [3] and Laser Doppler

Velocimetry (LDV) experimental data from Nouri et al. [4]. The unsteady forces obtained from this simulation are not directly helpful for GRTF studies. However this could be used as an input to a structural mechanics code. Experimentally, these forces can be measured by piezoelectric force transducers mounted on the wall. Axisa et al. [5] presented an interesting compilation of various experiments to study these random forces. It was observed that these random force fluctuations decrease with the frequency at which the force acts on the rod.

2. GEOMETRICAL CONFIGURATION UNDER STUDY

A concentric annular pipe with outer and inner diameter as 56.3 mm and 26.9 mm respectively was chosen as the computational domain. Water flows through the pipe in axial direction (z). A schematic diagram is shown in Fig. 1. Two mixing vanes were placed symmetrically inside the annulus at an inclination of 30° to the vertical axis. The orientation of the vanes can also be seen in Fig. 13. The dimensions of each vane were: length 17.9 mm, breadth 5.7 mm and thickness 1.2 mm. The ratio between the inner and outer radii defined as radius ratio of the pipe was 0.48 and the annular gap 14.7 mm. The hydraulic diameter, defined as $HD=4A_{\text{flow}}/P_{\text{wet}}$, was 0.03m where A_{flow} is the surface area of duct cross-section and P_{wet} is the wetted perimeter. The bulk velocity was 0.298m/s. Reynolds number based on the bulk velocity and hydraulic diameter was 8900. At a temperature of 20°C , the absolute or dynamic viscosity of water is $1.002 \times 10^{-3} \text{ Pa}\cdot\text{s}$ and the density is 998.2 kg/m^3 .

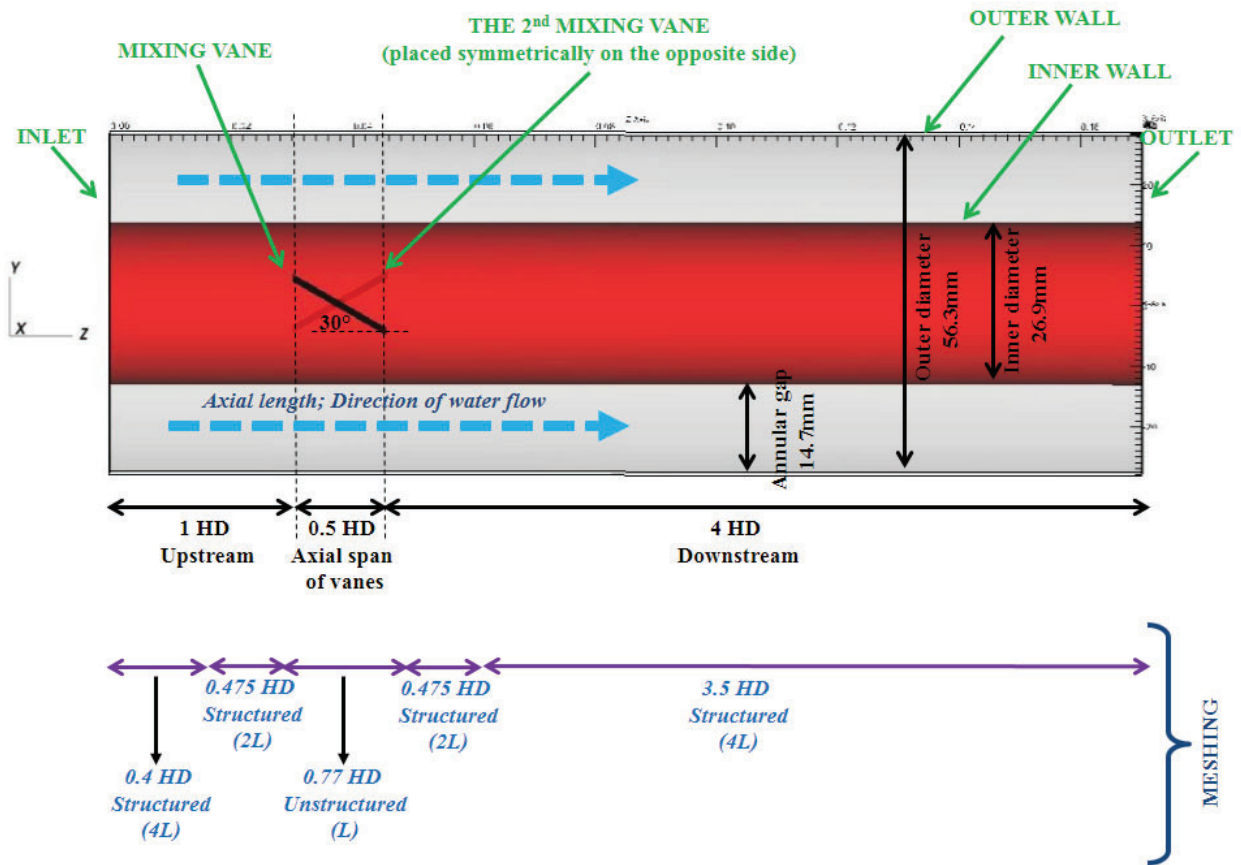


Figure 1. Schematic representation of the annular pipe

3. MESH GENERATION

In order to find a satisfying grid resolution for the computation, a mesh sensitivity study was carried out first without the vanes. Mesh was fully structured. Large eddy simulation (LES) was performed on the pipe with periodic axial boundary conditions for 5 different grid resolutions. Results were compared with DNS by Chung et al. [3] and a satisfying compromise was found between accuracy and computation cost. In terms of wall units, resolution of the order of 10 in axial, 3 in azimuthal and 1.3 in radial was found to be sufficient for reproducing the benchmark result. It was observed that the velocity profile was more affected by the azimuthal resolution than the axial resolution. Further details could be found in [6].

For the current computation, an attempt was made to keep the mesh structured as far as possible. However, the generation of structured mesh in the vicinity of vanes was not possible. So we decided to implement a hybrid mesh: unstructured mesh around the vanes and structured mesh in the rest of the domain. Tetrahedral mesh was generated with the CAD tool Gmsh [7]. Few mesh optimizations were carried out to improve mesh quality. In order to reduce the number of elements and computational cost, we implemented gradient stretching in axial direction keeping in mind the above grid resolutions [6]. Table I presents the grid resolution in wall units for the current simulation.

Table I. Grid resolutions

Boundary	Direction	Grid resolution	
		in wall units	in meters
Inner wall	Radial (<i>wall-normal</i>)	3.18	0.00030
	Azimuthal	3.18	0.00026
	Axial (<i>unstructured part</i>)	3.18	0.00030
	Axial (<i>structured part – the part with maximum stretching</i>)	12.72	0.00120
Outer wall	Radial (<i>wall-normal</i>)	2.98	0.00030
	Azimuthal	5.49	0.00055
	Axial (<i>unstructured part</i>)	2.98	0.00030
	Axial (<i>structured part – the part with maximum stretching</i>)	11.92	0.00120
Mixing vane	All directions	5.67	0.00030

The final domain comprised of 5 sub-domains (shown in Fig. 1):

- Unstructured sub-domain was created around the vanes with element size 0.0003m (in all 3 directions) bounded by structured inlet and outlet planes. This element size will henceforth be denoted as L . The resolution in terms of wall units was 5.67. The structured mesh on the inlet and outlet planes is shown in Fig. 3. The radial direction had uniform grid spacing ($=L$). In the azimuthal direction, the grid resolution was ~ 3 at the inner wall and ~ 5.5 at the outer wall.
- Using Gmsh, the inlet plane was extruded axially 0.475 times the hydraulic diameter (HD) with axial grid resolution of ~ 6 (wall units) to create the first upstream sub-domain.
- The second upstream sub-domain was similarly extruded 0.4 times HD axially using Gmsh with axial grid resolution of ~ 12 in wall units.
- The first downstream sub-domain was created by extruding the outlet plane 0.475 times HD using Gmsh with axial grid resolution ~ 6 in wall units.

- The second downstream sub-domain was similarly created by extruding the outlet plane 3.5 times HD using Gmsh with axial grid resolution ~ 12 in wall units.

The 5 sub-domains were joined together with Trio_U [8], maintaining the original mesh structure. A part of the final domain showing the hybrid mesh is presented in Fig. 2. The axial length of the domain was 0.17m, which corresponds to about 6 times the hydraulic diameter. The domain consisted of 19.36 million tetrahedrons. There were 50 grid points between the two walls.

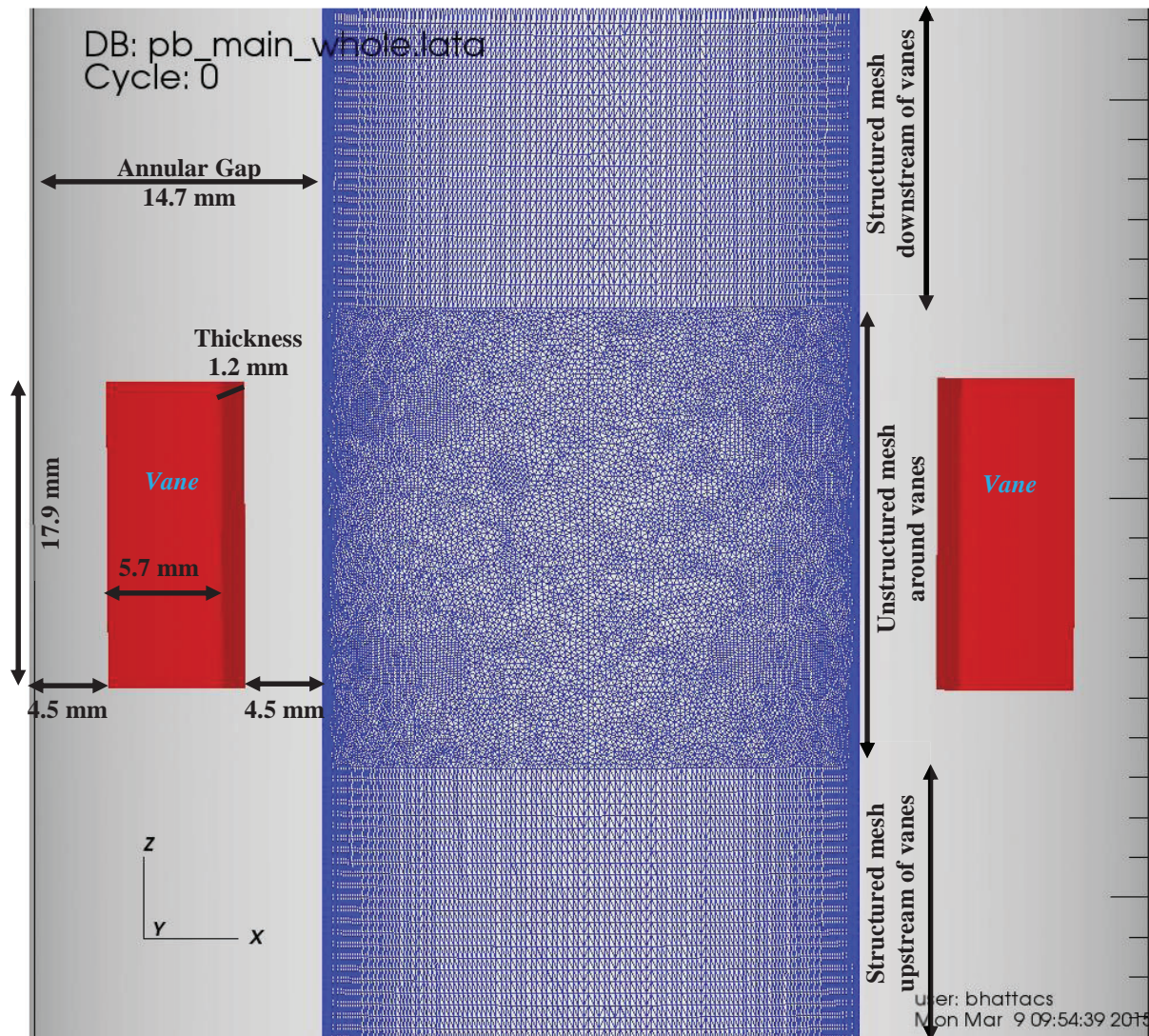


Figure 2. A section of the pipe showing hybrid structured and unstructured mesh

4. NUMERICAL METHODS

LES was used for modeling the turbulent flow in the annular pipe. LES uses spatial filtering to filter out small eddies and model them separately without explicitly solving them. The smaller eddies are nearly isotropic and show universal behavior and primarily dissipate kinetic energy [9]. The larger eddies are anisotropic and they efficiently transport the conserved properties and their behavior is dictated by

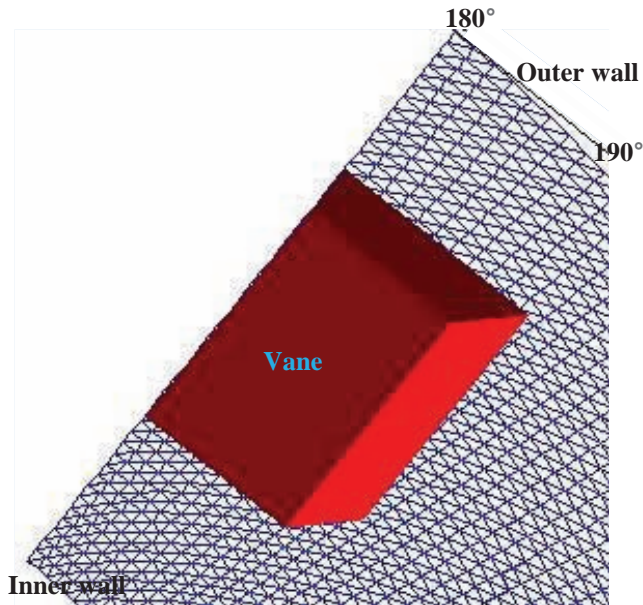


Figure 3. Structured mesh on the inlet and outlet surfaces

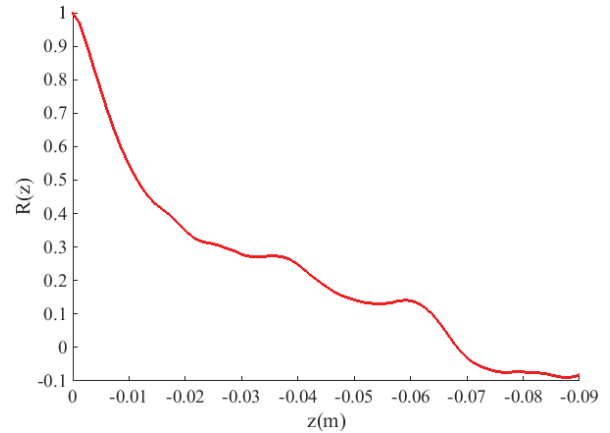


Figure 4. Two point correlation coefficient for axial velocity (periodic domain)

geometry, boundary conditions etc. A flow variable $\varphi(x, t)$ is split up as

$$\varphi(x, t) = \bar{\varphi}(x, t) + \varphi'(x, t) \quad (1)$$

where $\bar{\varphi}(x, t)$ is the filtered function with spatial variation greater than the filter cut off width (\sim grid cell size) and hence resolved by LES. $\varphi'(x, t)$ represents the unresolved spatial variation at length scales less than cut off width.

4.1. The Trio_U code

Trio_U [8] is a CFD code developed at CEA, France for unsteady, incompressible and compressible monophasic and diphasic flows. It is based on an object oriented, intrinsically parallel approach and is coded in C++. It uses a hybrid finite volume based finite element approach. This method involves determining for a continuous problem, a discrete solution in the space of the finite element by maintaining the balance notation of finite volumes [10]. The space discretization is performed with triangles in 2D and tetrahedrons in 3D. The main unknowns (velocity, temperature and concentration) are located at the center of the faces of an element (triangle or tetrahedron) whereas the pressure is discretized both at the center and at the vertices of the element. Trio_U uses a domain decomposition method for parallelization: the initial domain is decomposed into smaller overlapping sub-domains which are then distributed among the available processors. The processors communicate explicitly using MPI (message passing interface) libraries. Metis [11] partitioning tool was used to decompose the domain into 670 parts, i.e., 28800 elements per processor. For better performance, Trio_U recommends having 20000-30000 elements per processor.

4.2. Schemes

Space discretization was performed on the tetrahedral elements with the second order centered stabilized “EF_stab” scheme [12] and time discretization was done with second order explicit Adams-Bashforth scheme. The EF_stab scheme has a factor α to weigh the scheme centering between 0 (full centered) and

1 (mix between upwind and centered). Fully upwind schemes should be avoided for LES because they are too dissipative. [13] observed that $\alpha = 1$ tends to over dissipate the kinetic energy. Best practice guidelines for Trio_U [14] recommend the use of $\alpha=0.2$. Hence we used $\alpha=0.2$ which is in fact slightly upwind. The preconditioned conjugated gradient (GCP) iterative solver was used to solve the pressure matrix.

Various sub-grid scale models like the Smagorinsky-Lille model, WALE model, dynamic sub-grid scale model etc., exist for modeling the universal small scale eddies. The wall-adaptive local eddy viscosity (WALE) sub-grid scale model [15] was chosen because it goes naturally to zero at the wall, it has proper near wall scaling for eddy viscosity, and it correctly reproduces the laminar to turbulent transition. To fully resolve the large scale turbulent structures, grid resolution of the order of 1 is required near the wall. Since this wasn't the case, the Reichardt wall law [16] was used to model the near wall behavior.

4.3. Initial and boundary conditions

In order to have proper inlet boundary conditions quickly, a LES was performed on a domain extruded axially from the inlet plane of length 6 times the hydraulic diameter. During extrusion, the axial element length was maintained at $4L$ (same as in the second upstream and downstream sub-domains mentioned in Section 3). The domain consisted of 14 million tetrahedrons. Periodic boundary conditions were applied axially. A momentum source term was added to maintain constant mass flow rate. The axial length of the domain must be such that the two-point correlation coefficient goes to zero on half a period. Two point correlation coefficient $R(z)$ between the axial components of velocity is plotted in Fig. 4. The correlation falls to zero at separations suggesting that the domain is sufficiently long. The velocities obtained on the periodic boundary were injected at the inlet of the main domain at each time step. A constant pressure zero was imposed on the outlet boundary. No-slip boundary conditions were imposed on the inner and outer walls and the surface of the two vanes. In order to accelerate the formation of a physically correct solution, a fully turbulent flow developed in a separate periodic box was used as initial condition. This particular simulation was done on a relatively coarse mesh to save computational resource, while maintaining the same domain size.

5. RESULTS

LES was performed on 670 parallel processors of Curie supercomputer [17]. Initiating the simulation with a fully developed turbulent flow field saved significant computation time. The simulation was carried out for 2.5s physical time to collect sufficient statistics. This amounted to 77518 hours of CPU time on Curie. The calculation time step was 8×10^{-6} s; diffusive and convective time steps for the momentum equation were 9×10^{-6} s and 7×10^{-5} s respectively.

5.1. Velocity field

The statistics collected in the extruded periodic domain were first analyzed. Fig. 5 shows the mean axial velocity profile in the annular gap normalized by the bulk velocity (0.298m/s). It is in good agreement with the DNS of Chung et al. [3] performed at Reynolds number 8900. It reaches a maximum of 0.33m/s in the middle of the canal which corresponds to Reynolds number 9800. Fig. 6 shows the RMS distribution of fluctuating velocity. This was again normalized by bulk velocity in order to ascertain the reliability of the simulation by comparing with Nouri et al. [4]. The fluctuations reach a minimum at the middle of the hydraulic canal and peak close to the walls.

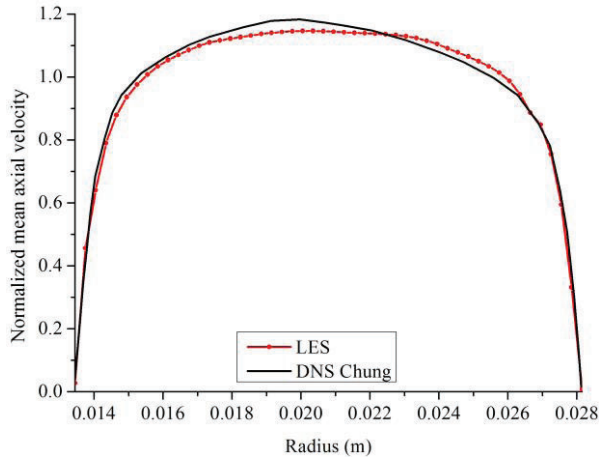


Figure 5. Mean velocity in periodic domain

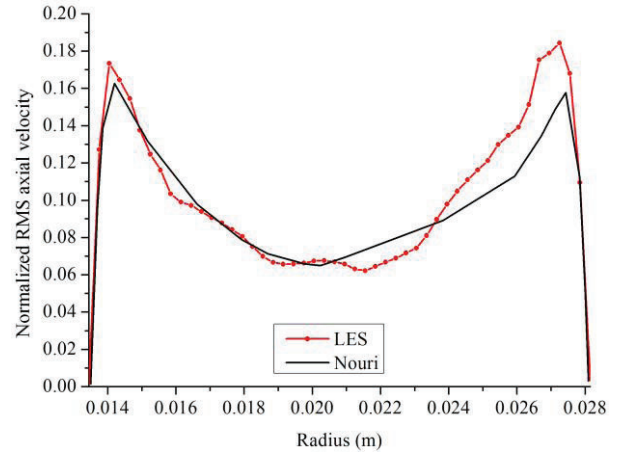
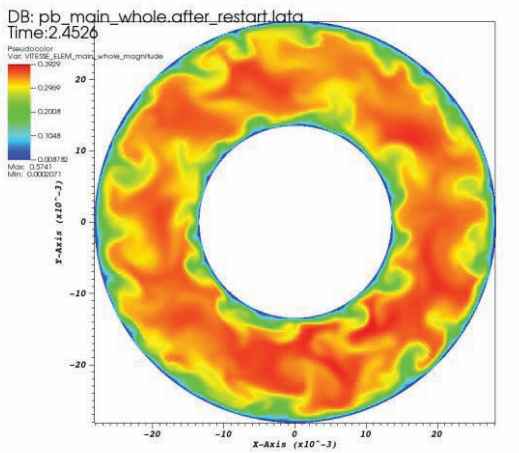
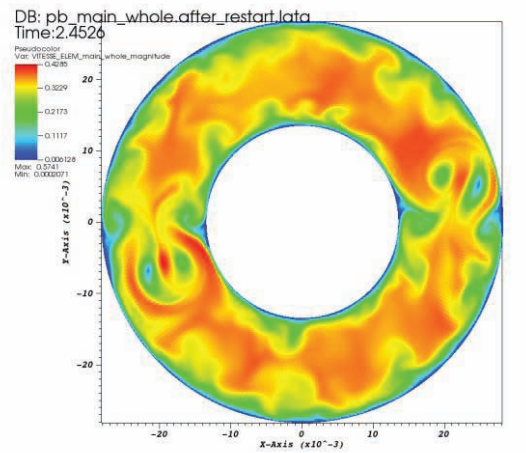


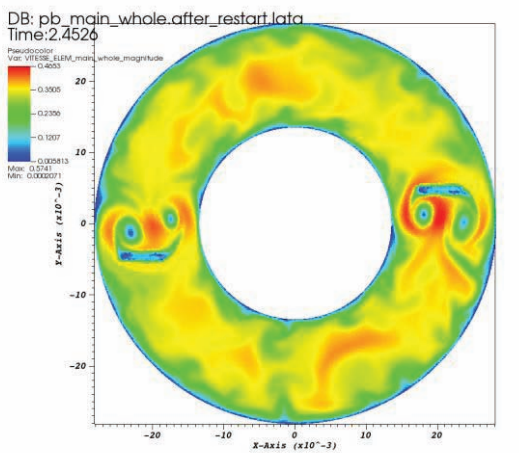
Figure 6. RMS velocity in periodic domain



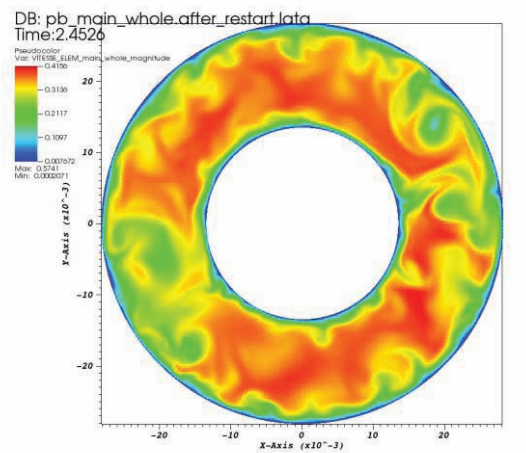
(a) 0.67HD upstream ($z=0.01\text{m}$)



(c) 0.8HD downstream ($z=0.07\text{m}$)



(b) 0.015HD downstream ($z=0.046\text{m}$)



(d) 2.8HD downstream ($z=0.13\text{m}$)

Figure 7. Instantaneous velocity on 2D planes at different heights in annular pipe

The instantaneous velocity field at different heights of the annular pipe is presented on 2D x-y planes in Fig.7 using VisIt [18]. The flow field shows a deviation in the flow pattern downstream of the vanes. This is because the vanes generate strong swirls in the annular gap. In a realistic nuclear reactor situation, the swirls increase heat transfer between the fuel rod cladding (the inner wall of the annulus) and the coolant (water).

At 0.67HD upstream of the vanes (Fig. 7a), the instantaneous velocity has a peak value 0.39m/s. The corresponding mean velocity profile is homogenous and has a value 0.36m/s at the middle of the hydraulic canal (Fig. 8). In Fig. 7b, immediately downstream of the mixing vanes (at 0.015HD), the velocity fluctuation in the vicinity of the vane is very large along the azimuthal direction: 0 - 0.45m/s. Further downstream at 0.8HD, the range reduces to 0.1 – 0.42m/s. At 2.8HD downstream of the vanes, the flow tends to homogenize with the velocity fluctuation ranging from 0.2 – 0.42m/s.

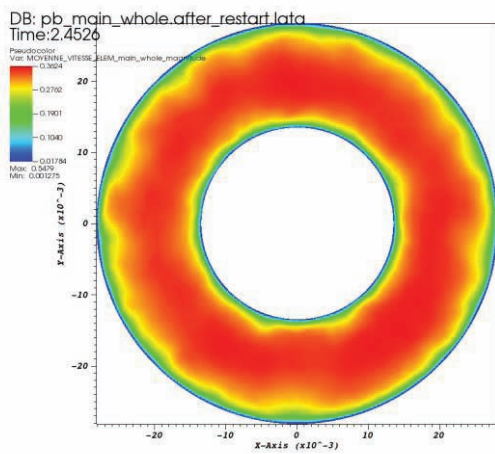


Figure 8. Mean velocity field at 0.67HD upstream ($z=0.01\text{m}$)

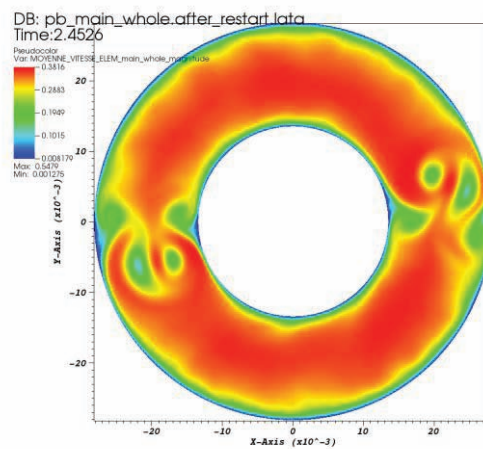


Figure 9. Mean velocity field at 0.8HD downstream ($z=0.07\text{m}$)

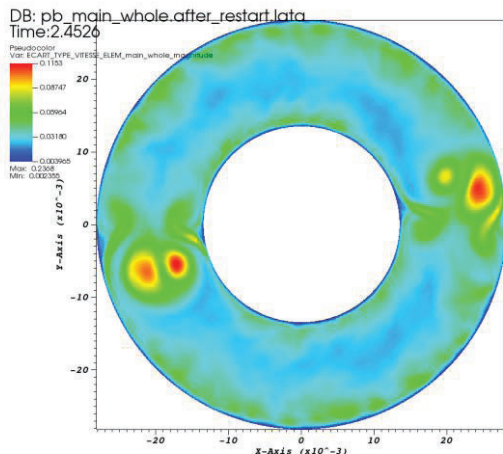


Figure 10. RMS velocity field at 0.8HD downstream ($z=0.07\text{m}$)

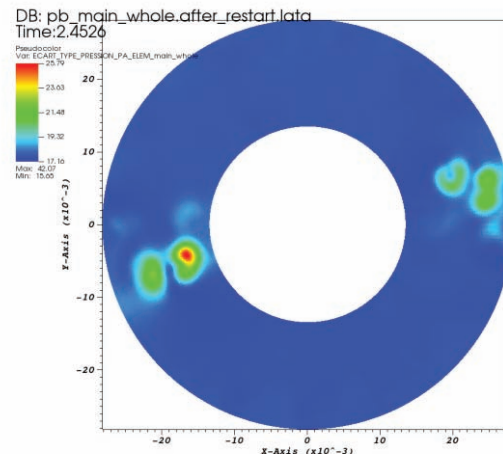


Figure 11. RMS pressure field at 0.8HD downstream ($z=0.07\text{m}$)

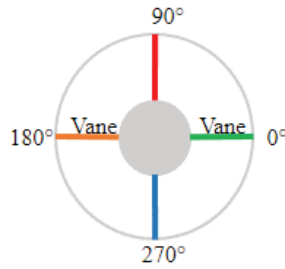


Figure 12 (a). Location of 4 probes placed on azimuthal plane at 0°, 90°, 180° and 270°

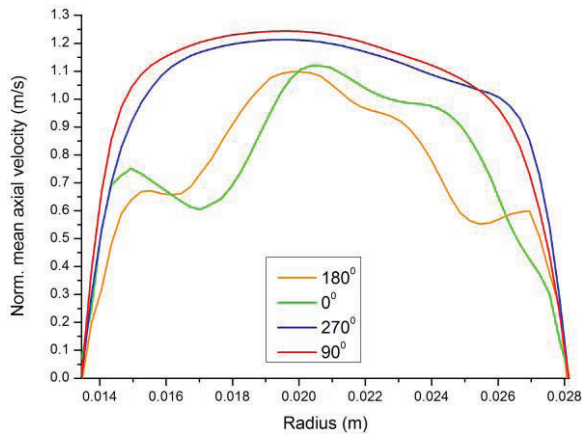


Figure 12 (b). Mean axial velocity profiles at 4 azimuthal locations

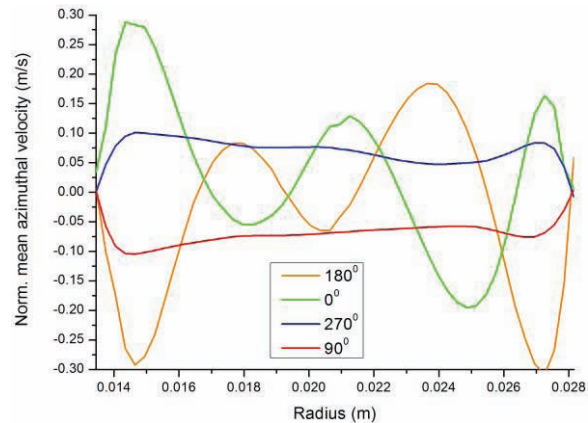


Figure 12 (c). Mean azimuthal velocity profiles at 4 azimuthal locations

Analysis of the velocity field at 0.8HD downstream of the vanes shows interesting results. The mean velocity at the middle of the canal is 0.38m/s. It seems that the mean velocity field is perturbed only in the vicinity of the vanes (Fig. 9). To see the effect of the vanes on the fluctuating field, RMS velocity and RMS pressure fields are plotted in Fig. 10 and 11 respectively. Clearly, one can observe strong fluctuation downstream of the vanes whereas it is homogenous in the rest of the canal.

It was also interesting to observe the same using mean velocity profiles at four locations as shown in Fig.12(a). Mixing vanes are at 0° and 180°. The mean velocity was normalized with the bulk velocity. In Fig.12(b), the profile of the axial component at 180° and 0° are significantly perturbed. In Fig.12(c), the azimuthal component too shows strong fluctuations downstream of the vanes. The peak at 180° and 0° is 3 times than that at 270° and 90°.

5.2. Analysis of lateral fluid forces on the rod

The inner wall of the pipe was divided into 17 equal rings of height 0.01m (which is equal to one-third of the hydraulic diameter HD) as shown in Fig. 13. The fluid force acting on the wall was calculated by integrating the pressure over the surface of each of these 17 rings. The x- and y- components of fluid force is responsible for the pressure force while the z-component is responsible for the viscous force. The contribution of viscous force is negligible compared to the pressure force [19].

Fig. 14 and 15 show the evolution of pressure force along the rod. The pressure force was integrated on a ring at every time step. These pressure force values were averaged over all time steps to obtain its mean

and RMS. The vertical dotted lines represent the axial bounds of the mixing vanes. The RMS of pressure force decreases downstream of the vanes implying a decrease in turbulent intensity. This was observed experimentally by [20].

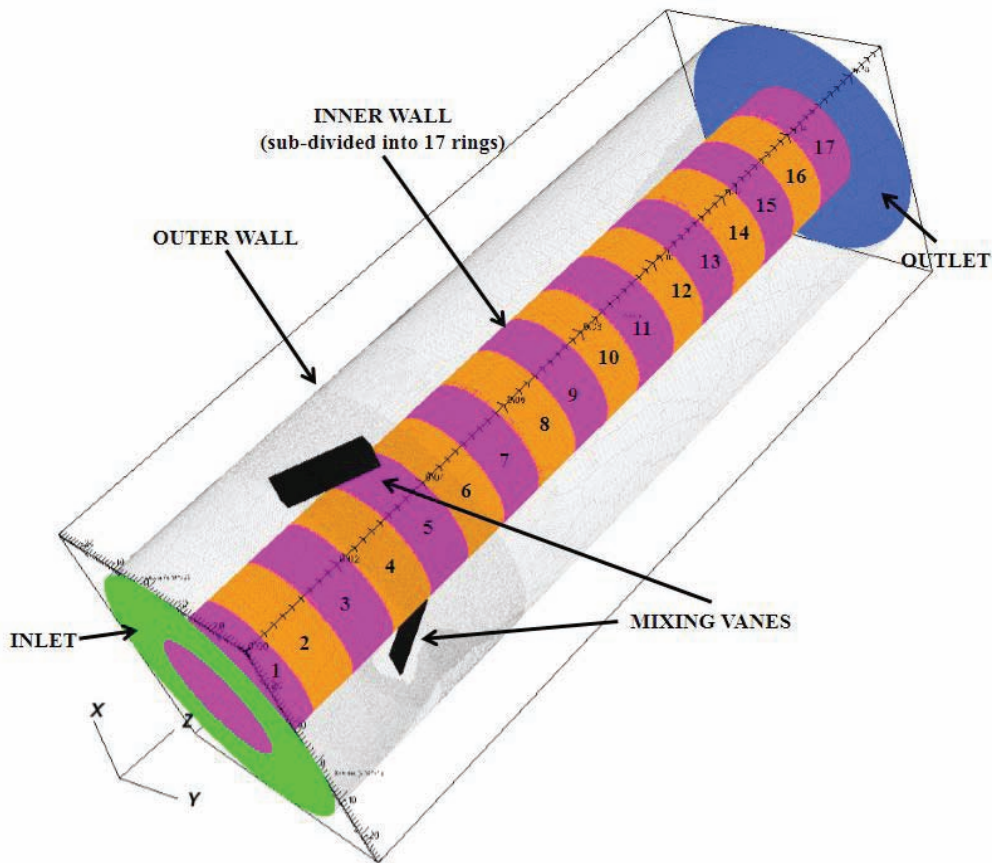


Figure 13. Inner wall divided into 17 equal rings

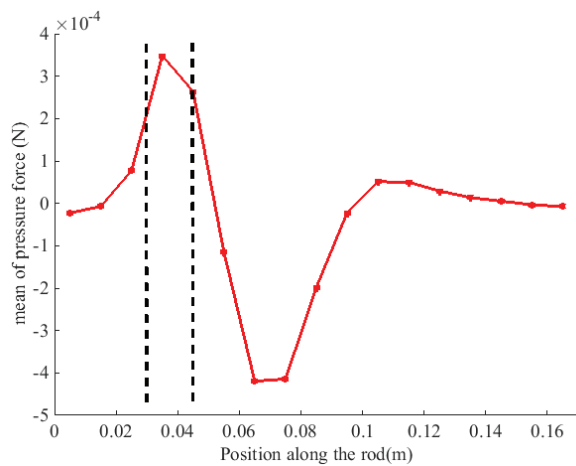


Figure 14. Mean pressure force along the rod

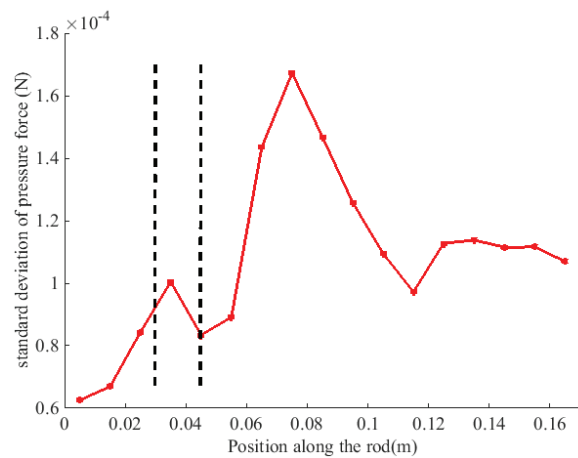


Figure 15. RMS pressure force along the rod

5.3. Pressure field

Since the hydrostatic pressure at the outlet is fixed at zero, the calculated inlet pressure determines the pressure drop over the whole domain. The pressure drop along the rod length is 16 Pa (Fig. 16). The pressure drop indicates that the bulk of the pressure loss is due to the mixing vanes. The spatial evolution of turbulent kinetic energy (TKE) is plotted in Fig. 17. It gives more information about the velocity field fluctuations. It peaks in the vicinity of the vanes. The maximum value of TKE occurs immediately downstream of the vanes.

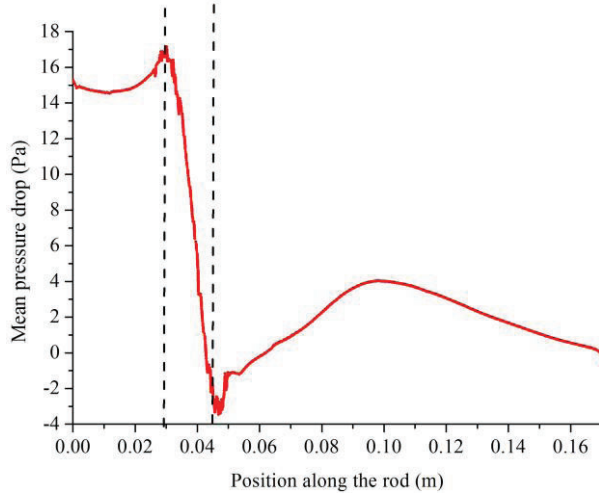


Figure 16. Mean pressure drop along the rod

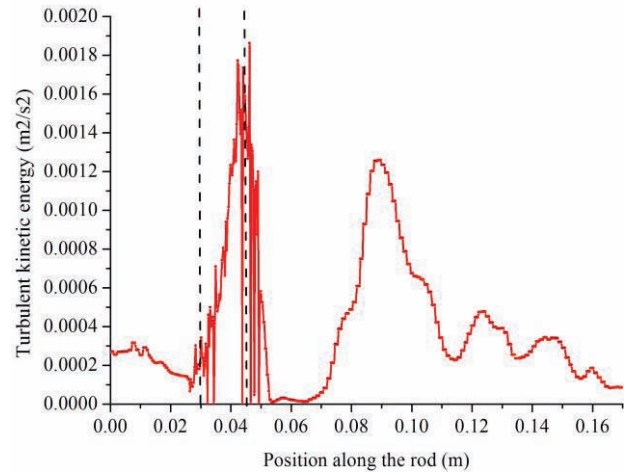


Figure 17. Variation of turbulent kinetic energy along the rod

Pressure fluctuation on the inner wall of the pipe were studied in terms of power spectral density. The PSD was rewritten in non-dimensional units as follows (presented in detail in [5]).

The reduced frequency is given by:

$$f_r = \frac{f \times D}{V_0} \quad (2)$$

The reduced power is given by:

$$PSD_r = \frac{PSD}{\rho^2 V_0^3 D} \quad (3)$$

where f denotes frequency in Hz, D is the external diameter of the rod under study (m), V_0 is average axial flow velocity in m/s, ρ is the fluid density in kg/m³ and PSD is the power spectral density of pressure in Pa²/Hz. In the current study, D represents the inner diameter of the annular pipe.

Fig. 18 shows the reduced power spectrum for pressure at 2 locations on the inner wall: one is 0.66HD upstream of vane ($z=0.01$ m) and the other is 0.8HD downstream of vane ($z=0.07$ m). The reduced frequency f_r is plotted on the horizontal axis and reduced power on vertical axis. It is observed that the fluctuations or amplitude of power decrease with frequency. Also at low frequencies, the power downstream is a decade higher compared to upstream.

Fig. 19 shows an angular distribution of mean pressure field at different heights on the inner wall of the pipe: -0.66HD, 0.16HD, 0.8HD, 1.8HD and 3.16HD. Maximum fluctuation is observed immediate downstream of the vanes at 0.16HD. Some fluctuations are also observed up to 0.8HD downstream. Beyond this, no pressure fluctuations are observed on the wall of the pipe.

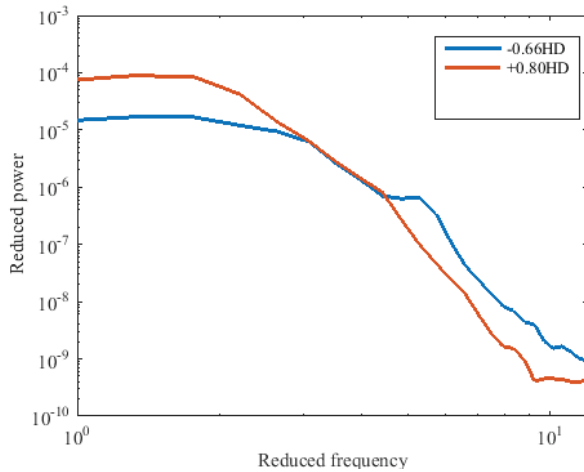


Figure 18. Reduced power spectrum for pressure at different heights

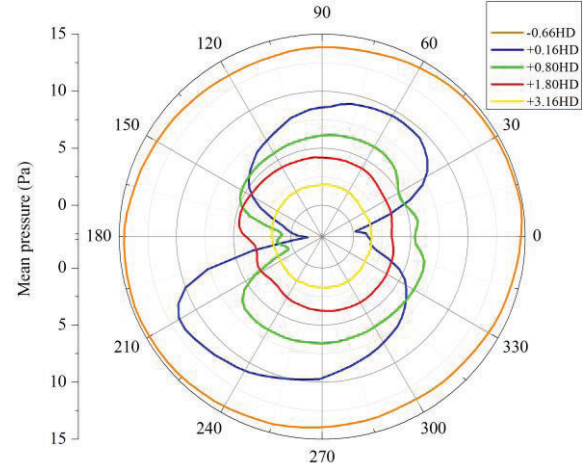


Figure 19. Azimuthal distribution of mean pressure at different heights of the inner wall

6. CONCLUSIONS

Large eddy simulations were carried out on a concentric annular pipe with mixing vanes with the CFD code Trio_U. The idea was to study the random fluctuating forces on the wall of the pipe due to the turbulent fluid flow. A hybrid structured-unstructured grid was used. Statistics of the fluctuating flow field were analyzed and compared to benchmark results. Velocity fields illustrate the swirl downstream of the vanes. The perturbations introduced by the vanes remain confined to the vicinity of the vanes as is seen from the RMS pressure and velocity fluctuations 0.8 hydraulic diameter downstream. It does not affect the flow field in other parts of the hydraulic canal. The pressure force exerted on the wall of the pipe was analyzed throughout the domain and it was observed that RMS fluctuations decrease downstream of the vane. Pressure fluctuations could be observed up to one hydraulic diameter downstream of the vanes.

The mesh sensitivity study was carried out without the vanes. Due to limitation of computation resource and time, a similar sensitivity study with the vanes could not be carried out for the moment. This would be done in the future to verify that the results do not change significantly. A sensitivity analysis of the resolution near the vanes would be performed in future to ascertain that the swirl structures downstream of the vanes are not affected by the grid resolution. Further sensitivity studies with respect to numerical schemes could be performed. For example, it would be interesting to see the effect of changing the coefficient α in the EF_stab space discretization scheme on the results with the same grid.

In Fig. 12(b) and 12(c), the slight asymmetry observed in the mean axial and mean azimuthal velocity profiles at 180° and 0° and at 270° and 90° might be due to convergence issues. Continuing the simulation for a much longer time would probably improve the results. This may also be attributed to the fact that the mesh pattern, being unstructured, is not the same on both sides.

ACKNOWLEDGMENTS

The authors would like to thank the Computing Center for Research and Technology (CCRT), Bruyères-le-Châtel, France for computation time on the Curie and Airain supercomputers. Further the authors would like to thank Areva and EDF for their support.

REFERENCES

1. “ADTSC Science Highlights”, Los Alamos National Laboratory, USA, <http://www.lanl.gov/orgs/adts/publications.php> (2013).
2. King, S.J., Young, M.Y., Seel, D.D., Conner, M.E., Lu, R.Y., Paramonov, D.V., “Flow induced vibration and fretting wear in PWR fuel,” *Proceedings of the 10th International Conference on Nuclear Engineering*, Arlington, VA, April 14 to 18 (2002).
3. Chung, S.Y., Rhee, G.H., Sung, H.J., “Direct numerical simulation of turbulent concentric annular pipe flow Part 1: Flow field”, *International Journal of Heat and Fluid Flow* **23**, pp.426-440 (2002).
4. Nouri, J.M., Umur, H., Whitelaw, J.H., “Flow of Newtonian and non-Newtonian fluids in concentric and eccentric annuli”, *Journal of Fluid Mechanics* **253**, pp.617-641 (1993).
5. Axisa, F., Antunes, J., Villard, B., “Random excitation of heat exchanger tubes by cross-flows,” *Journal of Fluid and Structures*, **4**, pp. 321-341 (1990).
6. Bhattacharjee, S., Ricciardi, G., Viazzo, S., “LES in a concentric annular pipe: Analysis of mesh sensitivity and wall pressure fluctuations”, *Proceedings of the ERCOFTAC Workshop Direct and Large Eddy Simulation 10 (DLES10)*, Limassol, Cyprus, May 27 to 29 (2015).
7. Geuzaine, C., Remacle, J.F., “Gmsh: a three dimensional finite element mesh generator with built-in pre- and post-processing facilities,” *International Journal for Numerical Methods in Engineering*, **79** (11), pp. 1309-1331 (2009).
8. “Trio_U - computational fluid dynamics code, version 1.7.0: French Alternative Energies & Atomic Energy Commission (CEA), France”, <http://www-trio-u.cea.fr> (2014).
9. Sagaut, P., *Large eddy simulation for incompressible flows*, Springer, Heidelberg (2005).
10. Bieder, U., Graffard, E., “Qualification of the CFD code Trio_U for full-scale reactor applications,” *Nuclear Engineering and Design*, **238**, pp. 671-679 (2008).
11. “METIS”, <http://glaros.dtc.umn.edu/gkhome/metis/metis/overview> (2013).
12. Kuzmin, D., Turek, S., “Multi-dimensional FEM-TVD paradigm for convection-dominated flows,” *Proceedings of ECCOMAS*, Jyvaskyla, 24-28 July, pp. 1-19 (2004).
13. Ducros, F., Bieder, U., Cioni, O., Fortin, T., Fournier, B., Fauchet, G., Quéméré, P., “Verification and validation considerations regarding the qualification of numerical schemes for LES for dilution problems”, *Nuclear Engineering and Design*, **240**, pp. 2123-2130 (2010).
14. Vandroux, S., Barthel, V., “Trio_U code validation database: Best practice guidelines: Technical note – CEA Saclay CEA/DEN/DANS/DM2S/STMF/LMSF/NT/13-008/A” (2013)
15. Nicoud, F., Ducros, F., “Sub-grid scale stress modeling based on the square of the velocity gradient tensor,” *Flow, turbulence and combustion*, **62**, pp. 183-200 (1999).
16. Hinze, J.O., *Turbulence*, McGraw-Hill, New York (1959).
17. “CCRT—Computing center for research and technology, France”, <http://www-hpc.cea.fr/en/complexe/tgcc-curie.htm>
18. “VisIt”: <https://wci.llnl.gov/simulation/computer-codes/visit/> (2014)
19. Delafontaine, S., Ricciardi, G., “Fluctuating pressure calculation induced by axial flow through mixing grid”, *Nuclear Engineering and Design*, **242**, pp. 233-246 (2012).
20. Caraghiaur, D., Anglart, H., Frid, W., “Experimental investigation of turbulent flow through spacer grids in fuel rod bundles”, *Nuclear Engineering and Design*, **239**, pp. 2013-2021 (2009).